ISSN 0915-633X

NATIONAL INSTITUTE FOR FUSION SCIENCE

Statistical Theory of L-H Transition in Tokamaks

S.-I. Itoh, K. Itoh and S. Toda

(Received - Jan. 8, 2003)

NIFS-771 Jan. 2003

TOKI, JAPAN

Statistical Theory of L-H Transition in Tokamaks

S -I. Itoh[1], K Itoh[2] and S Toda[2]

[1]Research Institute for Applied Mechanics, Kyushu University, Kasuga 816-8580, Japan
[2]National Institute for Fusion Science, Toki, 509-5292, Japan

Abstract

A statistical model for the bifurcation of the radial electric field E_r is developed in view of describing L-H transitions of tokamak plasmas. Noise in micro fluctuations is shown to lead to random changes of E_r, if a deterministic approach allows for more than one solution. The probability density function for and the ensemble average of E_r are obtained. The L-to-H and the H-to-L transition probabilities are calculated, and the effective phase limit is derived. Due to the suppression of turbulence by shear in E_r, the limit deviates from Maxwell's rule. The ensemble average of heat flux as well as that of E_r do not show a hysteresis in contrast to the deterministic model. Experimental condition for observing the hysteresis is also addressed.

Keywords: Statistical theory, L-H Transition, Tokamaks, Micro fluctuations, Hysteresis, Transition probability

1. Introduction

The formation of structures in inhomogeneous magnetized plasma has been one of the main issues in modern plasma physics. The strong turbulence, turbulent-driven transport and self-regulation of plasma profile take place through strong nonlinear interactions. An important example is the L-to-H-mode transition in toroidal plasmas [1, 2]. The key is the bifurcation of the radial electric field E_r [3, 4] and its mutual interaction with micro-scale turbulence [5, 6]. The micro-fluctuation has a micro scale length (such as the ion gyroradius ρ_i or collisionless skin depth $\delta = c/\omega_p$). The radial electric field, which is on a meso-scale (a hybrid mean between the characteristic scale length of the plasma radius a and micro-scales [7, 8]) including the zonal flow [9, 10], plays an essential role in the bifurcation and the suppression of the micro scale turbulence . Theory has made progress in explaining the existence of bifurcation in the radial electric field structure and the suppression of micro turbulence. (See reviews, e.g., [7, 11, 12].) Nevertheless, a further breakthrough is yet needed for understanding of the L-H transition phenomena. First, the statistical and stochastic properties of L-H transition must be clarified. This is because fluctuations and the mesoscale electric field are not at all in thermodynamical equilibrium. Phenomena evolve far from the laws of thermodynamical equilibrium. Efforts have been made for the far-non-equilibrium statistical law of micro turbulence [12-17], and the role of nonlinear noise source was found to be important. These analyses must be extended to cover the L-H transition phenomena. Also, an experimental test of theory is necessary. Experiments have shown recently that the change of radial electric field occurs in a very short time (a few times qR/c_s, where q is the safety factor, R: majour radius and c_s: ion sound velocity) [18] as has been predicted [3]. This supports the models implying hard bifurcation. On the other hand, a test of observing a hysteresis by use of a very slow change of parameters (on the scale of the energy confinement time or longer than that) could not identified clear hysteresis [19].

In preceding letter article [20], the statistical theory of the L-H transition has been discussed. In this article, we present a detailed description of the statistical model of the electric field bifurcation underlying the L-H transition in toroidal plasmas. Nonlinearity of micro-fluctuations statistically induces random noise in the meso-scale E_r. Being kicked by this random noise, transitions between the L- and H-states occur in a probabilistic manner. A Langevin equation can then be formulated including the mechanism for hysteresis of E_r. The probability density function (PDF) for and the ensemble average of E_r are obtained. The flux of probability density is calculated, and the transition probabilities between L-and H-states are found. The ensemble average of E_r does not show hysteresis in contrast to the deterministic model. The phase limit is given by the condition that the H- and L- states have equal probability. This implies an extension of Maxwell's rule. The phase limit shifts to the ridge of cusp for H-to-L

transition, due to the suppression of fluctuation by the shear in E_r. Whether the hysteresis is observed experimentally or not is shown to be determined by the competition between the life time (inverse of the transition rate) and the time for the change of global parameters. A condition that probabilistic transitions frequently occur is discussed.

The organization of this paper is in the following. In §2, Langevin equations as statistical equations are presented for microscopic fluctuation mode, for E_r which is on a meso scale and for the pressure gradient with a global scale. Section 3 is devoted to show the stationary solutions of the equations presented in §2 from a deterministic view point, discarding the stochastic noise source. Shown are the cases where a deterministic approach allows for more than one solution. Namely, the self-consistent solution of E_r contains hysteresis characteristics. Results from statistical analyses are given in §4. Stochastic noise sources are included by assuming a time scale hierarchy. PDF for E_r, and the L-to-H and H-to-L transition rates are obtained. The ensemble average of E_r and that of the heat flux are calculated and the effective phase limits are derived. Summary and discussions are given in §5.

2. Langevin equation

Understanding of the L-H transition mechanisms bas been in progress, and the interactions between the radial electric field structure, micro fluctuations and pressure gradient are now considered to play the key roles. (See reviews, e.g., [7, 11, 12].) They suppress and/or activate the others with strong nonlinearities. In the presence of microscale fluctuations, there arise random noise sources in the dynamics of larger scale structures due to nonlinearities. Both the averaged force and the statistical noise are to be included as the nonlinear effect of micro fluctuations. In this regard, we formulate Langevin equations of reduced variables for micro fluctuation mode, for the radial electric field which is on a meso scale, and for the global pressure gradient. To formulate the dynamical equations, we adopt a time scale hierarchy in the following. The characteristic times of the dynamics are

$$\tau_h \simeq a/c_s \ , \ \tau_X \simeq qR/c_s \ \text{ and } \tau_Y \simeq \ell^2/\chi_{N0} \ , \tag{1}$$

for micro fluctuations, the transition time of radial electric field and the evolution of pressure gradient, respectively. (The suffices h, X and Y are explained later. In equation (1), ℓ : characteristic radial scale length of E_r, and χ_{N0} : characteristic value of turbulent thermal diffusivity.) They are assumed to be well separated as $\tau_h << \tau_X << \tau_Y$.

For the convenience, we employ a normalization: a for length, $\tau_{tr} = 2qR/c_s$ for time, $\omega_{tr} = c_s/2qR$ for decorrelation rate, $V = c_s\left(a/2qR\right)$ for velocity,

$\Phi = aVB_0 = a\,c_s\left(a/2qR\right)B_0$ for electrostatic potential, $\bar{P} = B_0^2 R/2a\mu_0$ for plasma pressure, and $aV = a\,c_s\left(a/2qR\right)$ for diffusivity. (B_0 : magnetic field)

The derivation of the stochastic equation has been developed [21]. They are symbolically written as

$$\frac{\partial}{\partial t} f + \mathcal{L}^{(0)} f = \mathcal{N}\left(f, f\right) + \boldsymbol{Q}\ , \tag{2}$$

where $f^{\mathrm{T}} = \left(\phi,\ J_{\parallel},\ V_{\parallel},\ P_e,\ p_i\right)$ is the time-varying component of electrostatic potential, parallel current, parallel velocity, electron pressure and ion pressure, and $\mathcal{L}^{(0)} f$ represents the linear response. The term $\mathcal{N}\left(f, f\right)$ stands for the nonlinear terms $\mathcal{N}\left(f, f\right) = -\left(\nabla_{\perp}^{-2}\left[\phi,\ \nabla_{\perp}^2\phi\right],\ \left(1 - \xi\nabla_{\perp}^{-2}\right)^{-1}\left[\phi,\ J_{\parallel}\right],\ \left[\phi,\ V_{\parallel}\right],\ \left[\phi,\ P_e\right],\ \left[\phi,\ p_i\right]\right)$. The bracket $[f,g]$ denotes the Poisson bracket, $[f,\ g] = (\nabla f \times \nabla g)\cdot\boldsymbol{b}$, $\boldsymbol{b} = \boldsymbol{B}_0/B_0$ denotes the unit vector in the direction of the magnetic field and $\xi = \rho_i^2\delta^{-2}$. In the right hand side of equation (2), $\boldsymbol{Q}$ denotes the source terms, e. g., energy source or momentum source which might be constrained by external conditions. (The thermodynamical noise source $\tilde{S}_{th}$ could be kept in equation (2), if one studies the transition between thermodynamical fluctuations and turbulent fluctuations [15, 16]. It is not included in this article for the simplicity.) equation (2) describes micro fluctuations on the scale of τ_h, the evolution of E_r on the time scale of τ_X, the slow evolution of the order of τ_Y, the energy balance equation. equation (2) is solved for three dynamical components with time scales τ_h, τ_X and τ_Y.

The Lagrangean nonlinearity term $\mathcal{N}\left(f, f\right)$ gives three effects on a test mode f_k which is taken from the turbulent fluctuations. Part of the Lagrangean nonlinearity ($\mathcal{N}\left(f, f\right)$ for f_k) is coherent with respect to the test mode. This coherent part is considered to cause the turbulent drag, which is written as $-\Gamma_k f_k$. The second effect is the modification of the driving term. This is generated by the interaction of modes of different scale lengths, and is symbolically written as $\mathcal{D}_k f_k$. (A symbol 'D' stands for 'drive'.) The other incoherent part is considered as a random self-noise $\tilde{S}_k$. In order to describe the turbulence characteristics, we assume that the system has a large number of degrees of freedom and has many positive Lyapunov exponents. This assumption serves as a basis to treat the incoherent part $\tilde{S}_k$ as a rapidly varying random noise term. Symbolically, we write

$$\mathcal{N}_k\left(f, f\right) = -\Gamma_k f_k + \mathcal{D}_k f_k + \tilde{S}_k\ . \tag{3}$$

As has been discussed in [15, 16, 21, 22], a scale separation is introduced. In calculating the nonlinear drag term, fluctuations which have shorter wave-lengths are renormalized. One writes the nonlinear effects on the neighbouring modes (i.e., lower and higher modenumbers modes) as

$$\mathcal{N}^l(f, f) = -\left(\Gamma^l_{(l)} + \Gamma^l_{(h)}\right) f^l + \tilde{S}^l_{(l)} + \tilde{S}^l_{(h)} \tag{4a}$$

and

$$\mathcal{N}^h(f, f) = -\Gamma^h_{(h)} f^h + \mathcal{D}^h_{(l)} f^h + \tilde{S}^h_{(h)} , \tag{4b}$$

respectively. In this expression, the subscripts (l) and (h) denote the contributions from lower-modenumber modes and higher-modenumber modes, respectively.

The renormalized drag (coherent part) is given in a form of the eddy-viscosity type nonlinear transfer rate γ_j. A random-noise part is regarded to have a shorter decorrelation time than γ_j^{-1} according to rapid change model.[14, 23] The nonlinear drag term is written in a form of turbulent diffusivity as

$$\left(\Gamma f\right)^{\mathrm{T}} = \left(\mu_N \nabla_\perp^2 f_1, \mu_{N\parallel} \nabla_\perp^2 f_2, \mu_{Ne} \nabla_\perp^2 f_3, \chi_{Ne} \nabla_\perp^2 f_4, \chi_{Ni} \nabla_\perp^2 f_5\right) . \tag{5}$$

For micro fluctuations, it is simplified as $\left(\Gamma f\right)^{\mathrm{T}} = -\left(\gamma_1 f_1, \gamma_2 f_2, \gamma_3 f_3, \gamma_4 f_4, \gamma_5 f_5\right)$. The explicit form of the driving part is given in [21].

The same argument as above is applied to the other combination of perturbations with neighbouring scales. Therefore, more than three classes of modes with separated scale lengths are treated by the same procedure. Equations for E_r and global pressure gradient are also formulated as Langevin equations, in which the turbulent diffusion and nonlinear noises due to micro fluctuations are incorporated.

2.1 Micro mode

The microscopic fluctuation in turbulent plasmas has been studied intensively [12-17]. We adopt the result of the Langevin equation [15, 16] for the spectral amplitude of micro fluctuations as

$$\frac{\partial}{\partial t} I_h + \Lambda_h I_h = w(t) g_h \tag{6}$$

where $I_h = \phi_h^2$, (ϕ_h being the normalized electrostatic potential associated with microscopic fluctuations). The relation $\Lambda_h = 0$ gives the stationary solution of nonlinear dispersion relation in a deterministic analysis where

$$\Lambda_h = 2k_{h0}^2\left\{\sqrt{I_h} - D_h\right\} \tag{7}$$

with D_h being the transport coefficient by micromode, and k_{h0} is the characteristic wavenumber of microscopic fluctuations.

The parameter D_h, which is essential in determining the level of turbulence, has a dependence on the plasma parameters and the radial electric field. An explicit form differs by the choice of turbulent modes. If one employs example of the CDBM turbulence [7], one has explicit dependences as

$$D_h = \frac{G_0^{3/2}}{1 + \omega_E^2\tau_{ac}^2} s^{-2}\left(\frac{c}{a\omega_p}\right)^2 \tag{8a}$$

$$k_{h0}^2 \propto G_0^{-1}\left(1 + \omega_E^2\tau_{ac}^2\right) \tag{8b}$$

$$\bar{\Lambda}_h \propto G_0^{1/2}\left(1 + \omega_E^2\tau_{ac}^2\right)^0 , \tag{8c}$$

where G_0 is the normalized pressure gradient, s is the magnetic shear, ω_p is the plasma frequency, $\omega_E = B^{-1}\,\mathrm{d}E_r/\mathrm{d}r$ is the $E \times B$ shearing rate and τ_{ac} is the autocorrelation time of fluctuations [5, 7].

The right hand side of equation (6) denotes the statistical (stochastic) noise and g_h denotes the magnitude of the noise source and $w(t)$ is assumed to be the white noise.

The typical time scale of micromode is represented by the relaxation time of the amplitude. Let $I_h = \bar{I}_h + \delta I$, with $\sqrt{\bar{I}_h} = D_h$. The term Λ_h is expanded with respect to δI as

$$\Lambda_h = k_{h0}^2\left\{\sqrt{I_h} - D_h\right\} \simeq \frac{k_{h0}^2 D_h}{2\bar{I}_h}\,\delta I \ . \tag{9}$$

Then perturbation equation is given as

$$\frac{\partial}{\partial t}\,\delta I + \bar{\Lambda}_h \delta I = w(t) g_h \tag{10}$$

with

$$\overline{\Lambda}_h = k_{h0}^2 D_h \,, \tag{11}$$

showing that the characteristic time for the microscopic modes is $\overline{\Lambda}_h$, which gives $\tau_h \simeq a/c_s$ in diemnsional variables.

2.2 Radial electric field

We consider the case that a radial extent of ℓ characterizes the meso scale of the radial electric field E_r. The gradient is evaluated by $\mathrm{d}E_r/\mathrm{d}r \simeq E_r/\ell$. For this reduced variable E_r, a Langevin equation for the dynamics of the radial electric filed has been derived in [20] as

$$\frac{\partial}{\partial t} X + \Lambda_X X = w(t) g_X \tag{12}$$

where normalization is introduced for the electric field as

$$X = e\rho_p E_r / T \tag{13}$$

and ρ_p is the ion gyroradius at poloidal magnetic field and T is the plasma temperature. The damping term,

$$\Lambda_X X = \frac{qR}{\left(1+2q^2\right)\rho_s e c_s n_i} \bar{J}_r \tag{14}$$

is the normalized current. The source term Q in equation (2) for the radial electric field contributes to the radial current $\bar{J}_r$.

A specific form of Λ is chosen according to the model of L-H transition. Although there is no complete theoretical model that quantitatively explains the experimental observation as is tested in [24], D III-D observations supported the theories that had predicted the jump of E_r. Under this circumstance, let us consider a case of the E_r bifurcation where the bulk viscosity of ions, ion orbit loss and zonal flow excitation with shear viscosity damping have the key roles [3, 4, 10, 25]. One has

$$\Lambda_X X = \mathrm{Im}\, Z\left(X + i\nu_*\right) \cdot \left(X + X_{NC}\right) + \frac{\nu_b}{\left(\nu_b + \alpha X^4\right)^{1/2}} \exp\left(-\left(\nu_b + \alpha X^4\right)^{1/2}\right) + \gamma_{zonal} X \tag{15}$$

where $Z(X)$ is the plasma dispersion function, X_{NC} is the neoclassical drive and is of the order of normalized pressure gradient

$$Y = -\rho_p p_0^{-1} dp_0/dr , \tag{16}$$

$\nu_* = \nu_{ii} q R c_s^{-1}$ is the normalized ion collision frequency, $\nu_b = \varepsilon^{-3/2}\nu_*$, $\varepsilon = a/R$, α is a numerical parameter that denotes the orbit squeezing [4] and γ_{zonal} is the zonal flow excitation rate combined with shear viscosity damping [10]. We here employ a simplification $X_{NC} \simeq Y$. This simplification does not qualitatively affect the statistical property which is the subject of this article.

The radial current has two components: a time-averaged component, $\dot{J}_r$, and the rapidly-varying part J_r^n. The former, i.e., the time average-part (deterministic part) $\dot{J}_r$, has various origins including the bulk viscosity of ions, ion orbit loss, and eddy damping (or zonal flow excitation) for E_r by microfluctuations. The latter is induced by the convective nonlinearity in the vorticity equation $\tilde{V}\cdot\nabla\tilde{V}$ associated with micro fluctuations. It changes with the characteristic autocorrelation time of micro-fluctuations τ_{ac} , which is much shorter than the typical evolution time of E_r . In this article, the term J_r^n is considered to be a random noise. The time-average part $\dot{J}_r$ dictates the deterministic picture of bifurcations, and the noise part J_r^n gives a random kick for E_r and causes a probabilistic nature in transitions.

The magnitude of J_r^n is evaluated as follows. The nonlinearly-driven current, $J_r^n = m_i n_i B^{-1}\left\langle \tilde{V}\cdot\nabla\tilde{V} \right\rangle$ ($\langle\ \rangle$: averaged over the magnetic surface), is given as a sum of radial-Fourier components, $J_r^n = \sum_{d_z} J_r^n(d_z)$, where d_z is a radial wavelength of a randomly-excited current. One component is given as $\left|J_r^n(d_z)\right| = n_i m_i B^{-3} d_z^{-1} k_0^2 \tilde{\phi}^2$ for electrostatic fluctuations, where $\tilde{\phi}$ and k_0 are the amplitude of electrostatic potential perturbation and a characteristic wave number of micro-fluctuations, respectively. (When the finite-ion-gyroradius effect is included, $\tilde{\phi}$ is screened by a numerical factor.) Time-varying current $J_r^n(d_z)$ with various values of d_z can be simultaneously excited. Each d_z -component $J_r^n(d_z)$ is considered to be statistically independent, so that an average of the sum of $J_r^n(d_z)$ over the length ℓ is estimated as $\left|J_r^n\right| = \sqrt{\ell_z/\ell}\ \left|J_r^n(\ell_z)\right|$ after the law of large numbers, i.e., $\left|J_r^n\right| = n_i m_i B^{-3} \ell_z^{-1/2} \ell^{-1/2} k_0^2 \tilde{\phi}^2$. ($\ell_z$: a characteristic value of d_z .) The fact that J_r^n changes much faster than E_r enables us to approximate it as a white noise

$$J_r^{st} = n_i m_i B^{-3} \ell_z^{-1/2} \ell^{-1/2} k_0^2 \tilde{\phi}^2 \sqrt{\tau_{ac}}\, w(t) , \tag{17}$$

where $\sqrt{\tau_{ac}}$ is explicitly written for the dimension. (A detailed argument of modelling of noise term is given in [14, 17].) When τ_{ac} is much shorter than the response time of E_r , the statistical average of micro-fluctuations is calculated by treating E_r as a constant

parameter. In this dc-limit, fluctuation level has been given as $\left|\tilde{\phi}\right|^2 = \left(1 + \omega_E^2 \tau_{ac}^2\right)^{-1} \left|\tilde{\phi}\right|_L^2$, where $\left|\tilde{\phi}\right|_L^2$ is the fluctuation level in the L-mode state, $\omega_E = B^{-1}\, \mathrm{d}E_r/\mathrm{d}r$ is the $E \times B$ shearing rate.[5, 7] Using an evaluation $\mathrm{d}E_r/\mathrm{d}r \simeq E_r/\ell$, one has $\omega_E^2 \tau_{ac}^2 = \tau_{ac}^2 B^{-2} \ell^{-2} E_r^2$, or

$$1 + \omega_E^2 \tau_{ac}^2 = 1 + U X^2 \tag{18a}$$

with

$$U = \left(\hat{\tau}_{ac} a/\ell\right)^2 \tag{18b}$$

and $\hat{\tau}_{ac} = \tau_{ac} c_s / 2qR$. A magnitude of the noise source has been given as

$$g_X = \sqrt{\hat{\tau}_{ac}}\, \frac{R^2 k_0^2 \rho_i^2 \hat{\phi}^2}{a\sqrt{\ell\, \ell_z}}\, \frac{1}{1 + U X^2} \tag{19}$$

where $\hat{\phi} = e\left|\tilde{\phi}\right|_L / T$. In the following, $\left|\tilde{\phi}\right|_L^2$ and global plasma parameters (like temperature) are treated as control parameters.

2.3 Pressure gradient

For the slower time scale of τ_Y, equation (2) yields the energy balance equation

$$\frac{\partial}{\partial t} p_0 = \nabla \cdot \left(\chi \nabla p_0 - q_r\right) + \tilde{S}_E \tag{20a}$$

with the source $Q = -\nabla \cdot q_r$ and the thermal diffusivity

$$\chi = \chi_c + \chi_{turb}\,, \tag{20b}$$

where χ_c stands for the heat diffusivity due to the collisional process and χ_{turb} denotes that due to the turbulent transport process, q_r is the radial heat flux, and $\tilde{S}_E$ is a noise source for the global pressure from the fluctuations of the smaller scale length. The evolution of the pressure gradient is modelled from this equation (20). The evolution of the normalized pressure gradient $Y = -\rho_p\, p_0^{-1} \mathrm{d}p_0/\mathrm{d}r$ is modelled by

$$\frac{\partial}{\partial t} Y = \Delta \left(\chi Y - \frac{\rho_p}{p_0} q_r\right) + \tilde{S}_Y\,, \tag{21}$$

where $\tilde{S}_Y$ the noise source corresponding to $\tilde{S}_E$. Using the scale length ℓ, the operator is evaluated by $\Delta = \ell^{-2}$. With the normalized time $\tau = t\, c_s/2qR$, the Langevin equation of the pressure gradient is reduced to a point model

$$\frac{\partial}{\partial \tau} Y + \Lambda_Y Y = w(t) g_Y , \tag{22}$$

where the damping term coefficient is expressed as

$$\Lambda_Y = \gamma_c + \gamma_{turb} - P_{in} Y^{-1} \tag{23}$$

with the normalized rates and heat flux as

$$\gamma_c = \frac{2qR}{c_s} \frac{\chi_c}{\ell^2} , \quad \gamma_{turb} = \frac{2qR}{c_s} \frac{\chi_{turb}}{\ell^2} \quad \text{and} \quad P_{in} = \frac{2Rq}{c_s \ell^2} \frac{\rho_p}{p_0} q_r . \tag{24}$$

In equation (23), P_{in} is the parameter that characterizes the magnitude of heat flux. (A brief explanation of the normalization is made; γ_{turb} and γ_c are turbulent and collisional diffusion rates normalized to the ion-sound transit time qR/c_s. Normalization of the heat flux, $p_0 c_s \ell^2/2Rq\rho_p$, is a characteristic Bohm-diffusion flux $c_s \rho_i p_0/a$ being multiplied by a geometrical factor $\ell^2/2\rho_p^2$.)

The turbulent heat flux χ_{turb} depends on the pressure gradient and the gradient of radial electric field. The driving parameter G_0 is rewritten as $G_0 = \left(a \frac{\mathrm{d}}{\mathrm{d}r} \ln B_0\right) \frac{a^2 \beta}{R\rho_p} Y$. For the case of CDBM turbulence, it takes the form

$$\chi_{turb} = \frac{\chi_{N0} Y^{1.5}}{1 + UX^2} , \tag{25a}$$

or

$$\gamma_{turb} = \gamma_{N0} \frac{Y^{1.5}}{1 + UX^2} . \tag{25b}$$

Normalized coefficients are given as

$$\gamma_{N0} = \chi_{N0} 2qR/c_s \quad \text{and} \quad \chi_{N0} = \left(a \frac{\mathrm{d}}{\mathrm{d}r} \ln B_0 \frac{a^2 \beta}{R\rho_p}\right)^{3/2} s^{-2} \left(\frac{c}{a\omega_p}\right)^2 . \tag{26}$$

2.4 Set of Langevin equations

The set of Langevin equations is derived as equations (6), (13) and (22). Equations

$$\frac{\partial}{\partial t} I_h + \Lambda_h I_h = w(t) g_h$$

$$\frac{\partial}{\partial t} X + \Lambda_X X = w(t) g_X$$

$$\frac{\partial}{\partial \tau} Y + \Lambda_Y Y = w(t) g_Y$$

form a basis of the analysis.

Note that there is a difference in a time scale;

$$\bar{\Lambda}_h >> 1 \ , \ |\Lambda_X| \sim O(1) \ , \ |\Lambda_Y| << 1 \ .$$

Time scale separation: time-scale hierarchy

$$|\bar{\Lambda}_h| >> |\Lambda_X| >> |\Lambda_Y| \tag{27}$$

is understood that characteristic times of dynamics are

$$\tau_h \simeq a/c_s \tag{28a}$$

for micro fluctuations,

$$\tau_X \simeq qR/c_s \tag{28b}$$

at the transition of electric field, and

$$\tau_Y \simeq \ell^2/\chi_{N0} \ ; \tag{28c}$$

for the evolution of the pressure gradient. For Bohm-like transport, one has $\tau_Y \simeq \frac{a}{\rho_i}\frac{a}{c_s}$.

One has a relation

$$\tau_h << \tau_X << \tau_Y \tag{29}$$

i.e., equation (27), for typical parameters of tokamak plasmas.

By employing this time-scale hierarchy, statistical property of the system (I_h, X, Y) is studied. In solving dynamics of micro mode, global parameters X and Y are treated as constant parameters. (Adiabatic approximation) This process has been analyzed in preceding articles, and statistical average $\langle I_h \rangle$ has been obtained.[15]

A couple of models has been proposed to study the dynamics of the L-H transition. A set for the fluctuation level, electric field inhomogeneity and pressure gradient has been given in [26]. Other models with soft bifurcations are given in [27]. The case with hysteresis has been proposed in [8]. The previous models are devoted to the discussion based upon the deterministic view without a noise contribution. However, this set of equations (6), (13) and (22) includes the statistical noises so that the statistical and stochastic description is available in the bifurcation dynamics. In the following, an analysis of the deterministic picture is first explained in §3. Then the statistical analysis is developed in §4.

3. Solution of deterministic picture

Stationary solutions in the deterministic view without a noise is obtained from the nonlinear dynamic equations

$$\Lambda_h = 0 , \tag{30a}$$

$$\Lambda_X = 0 , \tag{30b}$$

and

$$\Lambda_Y = 0 . \tag{30c}$$

One of the solutions of equation (30a) for CDBM is given by equation (8). In the following, the solutions of equations (30b) and (30c) along with equation (8) are discussed as an example case.

3.2 Electric field structure

Equation $\Lambda_X = 0$ means that

$$\mathrm{Im}\, Z(X + i\nu_*) \cdot (X + Y) = -\frac{\nu_b}{(\nu_b + \alpha X^4)^{1/2}} \exp\left(-(\nu_b + \alpha X^4)^{1/2}\right) \tag{31}$$

holds. For given parameters (ν_b, Y), this is a nonlinear equation of X and has either one solution of X or three solutions of X. For a fixed value of ν_b, $\nu_b = 0.5$, the

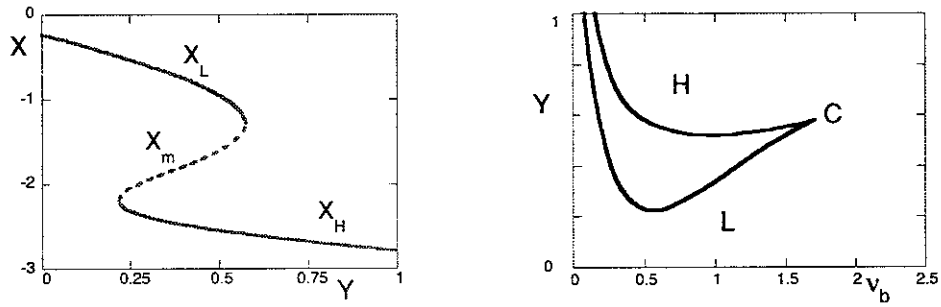

Figure 1 (a) The electric field solution X as a function of the normalized gradient Y for a fixed value of ν_b ($\nu_* = 0.1$). (b) Phase diagram of the radial electric field solution in the space of (ν_b, Y) . The result of the deterministic analysis, $\Lambda_X = 0$. (Parameters are: $\alpha = 0.5$, $q = 3$, $\varepsilon = a/R = 1/3$.)

solution X is illustrated as a function of Y in figure 1(a). When there are three solutions, we call them X_L , X_m and X_H . (The intermediate solution X_m is unstable.) "L" is the low confinement region, and "H" stands for the high confinement region. When the value of ν_b changes, the characteristic curve changes. At $\nu_b \simeq 1.7$, the H-branch and L-branch merge. The phase diagram of X on (ν_b, Y) plane is shown in the figure 1(b). A cusp catastrophe is shown. "C" (where $\nu_b \simeq 1.7$ holds) denotes the critical point. In the cusp region three branches of solutions exist, two of which are stable.

3.3 Pressure gradient

The nonlinear relation for the normalized pressure gradient Y , $\Lambda_Y = 0$, provides another relation between the electric field and pressure gradients. This equation is rewritten as

$$\left(\gamma_c Y + \frac{\gamma_{N0} Y^{2.5}}{1 + UX^2}\right) = P_{in} \ . \tag{32}$$

For a fixed heating power $P_{\rm in}$, X as a function of Y is shown in the figure 2(a). (Parameters are $P_{in} = 0.01$, $\gamma_c = 0.01$, $\gamma_{N0} = 0.5$ and $U = 3$. Small normalized values of P_{in} comes from the relation $|\Lambda_Y| << 1$.)

The limiting form of the solution of Y for small X and large flux P_{in} is

$$Y = Y_L \equiv \left(\frac{P_{in}}{\gamma_{N0}}\right)^{0.4} , \tag{33a}$$

and that in the limit of large X is given as

$$Y = Y_c \equiv \frac{P_{in}}{\gamma_c} . \tag{33b}$$

In equation (33a), Y_L corresponds to the gradient in the absence of the electric field shear stabilization, and in equation (33b), Y_c is the pressure gradient in the absence of the turbulent transport, respectively.

Let us study the variation from Y_L to Y_c. For a various heating power, the solution $X(Y)$ of $\Lambda_Y = 0$ is illustrated in figure 2(b). For a small heat flux, $P_{in} < \gamma_c^{5/3}\gamma_{N0}^{-2/3}$, the curve is close to a vertical line $Y \simeq Y_L \simeq Y_c$. As P_{in} increases, the curve $X(Y)$ is inclined more strongly. Note that the sign of X is negative.

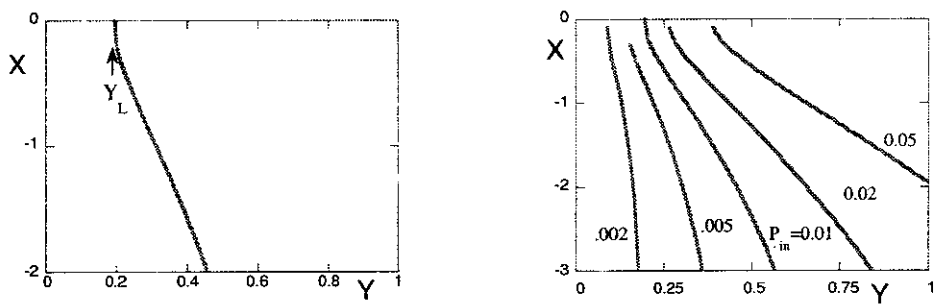

Figure 2 (a) The solution of $\Lambda_Y = 0$ for $P_{in} = 0.01$,. $\chi_{N0}/\chi_c = 50$. (b) Solution of $\Lambda_Y = 0$ for various values of P_{in}. (Paremeters are: $\gamma_c = 0.01$, $\gamma_{N0} = 0.5$ and $U = 3$).

3.4 Self-consistent solution

Self-consistent solutions must satisfy all the conditions of $\Lambda_h = 0$, $\Lambda_X = 0$ and $\Lambda_Y = 0$. They are obtained in the following. (Those with trivial solutions $I_h = 0$ are not discussed in this article.) Figure 3 illustrates the curves of $\Lambda_X = 0$ and $\Lambda_Y = 0$ on the (X, Y) plane simultaneously, so that the cross points are the self-consistent solutions. For a weak hating power, $P_{in} < 0.0023$ for the parameters of the figure 3, there is only one solution in the branch of X_L. In an intermediate regime, $0.0023 < P_{in} < 0.03$, three branches of solution are possible. In a case of strong heating power, $P_{in} > 0.03$, one branch of solution, X_H , exists.

The heat flux as a function of the gradient is calculated for these self-consistent solutions. In the deterministic model, a hysteresis appears in the gradient-flux relation. Figure 4 shows a cusp type relation of the heat flux as a function of the gradient. Thick lines are for the total flux. Thin dotted line indicates the contribution of the collisional

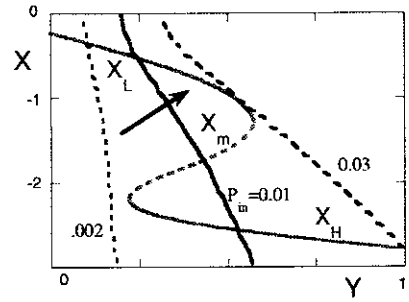

Figure 3 Solution of $\Lambda_X = 0$ (a thick curve with hysteresis) and that of $\Lambda_Y = 0$ (thin lines, $P_{in} = 0.002$, 0.01 and 0.03). The crossing points represent the self-consistent solution of the stationary state in the deterministic view. Arrow indicates the increment of $P_{\rm in}$. (Parameters are: $\alpha = 0.5$, $q = 3$, $\varepsilon = a/R = 1/3$, $U = 3$.)

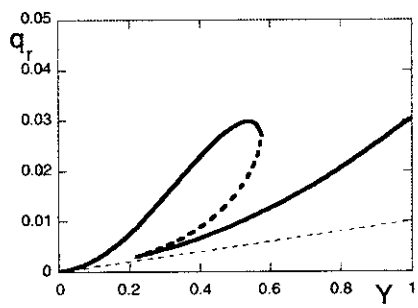

Figure 4 Heat flux in the vertical axis is measured in the unit of $c_s \ell^2 p_0 / 2Rq\rho_p$. Thick lines are for the total flux. Thin dotted line indicates the contribution of the collisional transport. (Parameters are: $\alpha = 0.5$, $q = 3$, $\varepsilon = a/R = 1/3$, $U = 3$.)

transport. The ridge point of this hysteresis depends on the collisionality and is illustrated in the figure 1.

4 Statistical picture

In the presence of the noise, the statistical and stochastic description of the problem is inevitable, if a deterministic approach allows for more than one solution. The transition rate between different branches are to be evaluated. Based on this, the statistical ensemble average and the variance of the heat flux are discussed.

In this section, we study the L/H transition, focusing to the dynamics of the variable X . The required time scale hierarchy among three variables of I_h , X and Y is discussed (§4.1). Then the probability density function (PDF) is obtained in relation with the noise source (§4.2). Transition probability can be evaluated by means of transition rate (§4.3). Long time average and ensemble average are then obtained as the statistical-

average values (§4.4). The limit (boundary) is drawn in the phase diagram. The relation between phase limit and the conventional Maxwell's rule is discussed (§4.5). The condition for observing hysteresis in experiments is discussed (§4.6).

4.1 Time scale hierarchy

In analyzing the dynamics of radial electric field X, global parameter Y is considered as constant, and the micro-mode is replaced by its statistical average $\langle I_h \rangle$. The dynamics of Y are solved by introducing statistical averages of X and micromode I_h. This is due to the time scale hierarchy previously introduced in the previous section (§2.4), i.e., equation (27),

$$|\bar{\Lambda}_h| >> |\Lambda_X| >> |\Lambda_Y| .$$

The statistical transition is possible for system with the hysteresis characteristics of the radial electric field. Stationary solutions which satisfy $\Lambda_X = 0$ and $\Lambda_Y = 0$ are shown by the crossing points of curves in figure 5. Let us study the temporal evolution on this plane in the following. First, the evolution from the neighborhood of A is considered. Both the transition from A to A' and the back-transition from A' to A take place, because the change of the radial electric field is much faster than the variation of Y. The equilibration between A and A' is reached. If A is much more probable than A', the evolution of Y does not occur and the state A is the stationary state. If A' is more probable than A, the transition to the branch $X \simeq X_H$ happens, and then the change from A' to B occurs along the path of $X \simeq X_H$.

Next, the evolution from B is studied. The equilibration between B and B' takes place much faster than the change of Y. When the state B' is more probable than B, the jump from B to B' takes place and the transition to the branch $X \simeq X_L$ occurs. It is followed by the slow evolution from B' to A along the path of $X \simeq X_L$.

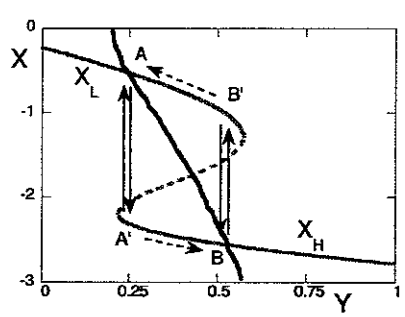

Figure 5 Adiabatic limit of transition and path of evolution.

The transition process is analyzed by calculating the transition rate between branches X_L and X_H for fixed value of Y. In the process of the jump of X, the micro-fluctuations are considered to reach their long-time statistical average.

4.2 Probability density function (PDF)

Statistical property of the radial electric field is described by use of the probability density function (PDF) of X, $P(X)$. Based on the adiabatic approximation, equation (27), X varies much faster than Y but slower than I_h. Therefore the equation for PDF of the variable X is formulated with a fixed value of Y and statistical average of I_h, which is governed by the Fokker-Planck equation

$$\frac{\partial}{\partial \tau} P + \frac{\partial}{\partial X}\left(\Lambda_X + g_X \frac{\partial}{\partial X} g_X\right) P = 0 \ . \tag{34}$$

The stationary solution $P_{st}(X)$ for $\partial/\partial t = 0$ is obtained from a conventional approach of statistical physics and expressed as

$$P_{st}(X) = \bar{P}_{st}\, g_X^{-1} \exp\left(-S(X)\right) \tag{35}$$

with the nonlinear potential defined as

$$S(X) = \int^{X} \frac{4\Lambda_X(X')X'}{g_X(X')^2}\, dX' \ , \tag{36}$$

where $\bar{P}_{st}$ is a normalization constant. In performing the integral with respect to X in equation (36), Y is kept constant (the path like $A - A'$ in figure 5).

The dominant parameter dependence of $P_{st}(X)$ comes from $\exp\left(-S(X)\right)$, where

$$-S(X) = \Gamma \int_0^{X} \Lambda_X X' \left(1 + UX'^2\right)^2 dX' \tag{37}$$

with

$$\Gamma = 2\, \hat{\tau}_{ac}^{-1} a^2 \ell\, \ell_z R^{-4} k_0^{-4} \rho_i^{-4}\, \hat{\phi}^{-4} \ . \tag{38}$$

The minimum of $S(X)$, i.e., zero of Λ_X (apart from a correction ln g), predicts the most probable state of X. $S(X)$ can have two minima at $X = X_L$ and $X = X_H$, which are

separated by the local maximum at $X = X_{\rm m}$. When two minima exist, the L-H transition has a hysteresis in a deterministic description. In this case, (i.e., the cusp region of figure 1(b)), $S(X)$ has the maxima at

$$X = 0 \text{ and } X = X_m , \tag{39a}$$

where $X = 0$ corresponds to a branch only with a thermal fluctuations, and has the minima at

$$X = X_L \text{ and } X = X_H . \tag{39b}$$

The potential function $S(X)$ is illustrated in figure 6 for the case with a hysteresis. The thick solid line, $Y = 0.4$ is the case where the minima of $S(X)$ take nearly equal values, $S(X_{\rm L}) \simeq S(X_{\rm H})$. Below this critical pressure gradient with fixed collisionality, the relation $S(X_{\rm L}) < S(X_{\rm H})$ holds (thin dotted line, $Y = 0.38$) and the branch $X = X_L$ is dominant. At higher pressure gradient, the relation $S(X_{\rm L}) > S(X_{\rm H})$ holds for fixed collisionality (thin broken line, $Y = 0.42$), and the branch $X = X_H$ is dominant.

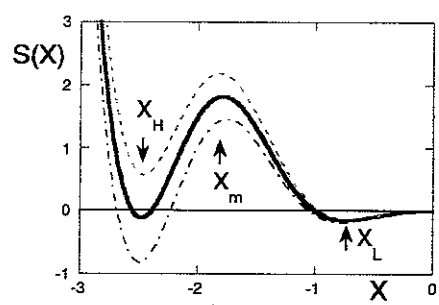

Figure 6 Nonlinear potential function $S(X)$ for various values of the pressure gradient Y . $Y = 0.4$ for the solid line, $Y = 0.38$ for the thin dotted line, and $Y = 0.42$ for the thin broken line. Two minima, $X = X_L$ and $X = X_H$, and two maxima, $X = 0$ (branch with only a thermal fluctuation) and $X = X_m$, are seen. (Other parameters are fixed as $U = 3$, $\Gamma = 5$ and $\nu_* = 0.1$.)

Probability density function for the stationary solution $P_{\rm st}(X)$ is illustrated in figure 7 for the conditions of figure 6. The case where two branches of $X = X_L$ and $X = X_H$ have nearly equal probabilities is shown by the solid line ($Y = 0.4$). The dotted line indicates the case that the branch $X = X_L$ is dominant ($Y = 0.38$), and the broken line

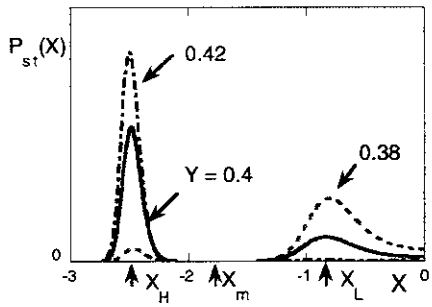

Figure 7 Probability density in a stationary state in the adiabatic limit of fixed value of Y. Lines correspond to those in figure 6. $Y = 0.4$ for the solid line, $Y = 0.38$ for the thin dotted line, and $Y = 0.42$ for the thin broken line.

shows that the branch $X = X_H$ is dominant ($Y = 0.42$). In these three cases, the hysteresis exists and the bistable solutions are given. However, it is seen that, depending on the depth of the potential function $S(X)$, the probability being in one branch or in the other can be strongly different.

The parameter Γ, being in proportion to $\langle I_h \rangle^{-2}$, denotes the width around the peak of PDF. The widths become narrower, if the turbulence level $\langle I_h \rangle$ is low and Γ is large. When the turbulence level increases, Γ becomes smaller and the width around the peak of PDF turns broader. In figure 7, the width of the peak at $X = X_H$ is narrower than that at $X = X_L$ for a given value of Γ. This is because the fluctuations are suppressed due to the shear in E_r becomes stronger.

4.3 Transition rate

The transition rate is obtained from the Fokker-Planck equation (34). Calculating a flux of probability density by a conventional procedure, it is expressed by use of the potential $S(X)$.[16, 28] The rates of the L-to-H transition and the back-transition (H-to-L transition) are obtained as

$$r_{\mathrm{L}\to\mathrm{H}} = \frac{\sqrt{\Lambda_{\mathrm{L}}\Lambda_{\mathrm{m}}}}{2\pi} \exp\left(S(X_{\mathrm{L}}) - S(X_{\mathrm{m}})\right), \tag{40a}$$

$$r_{\mathrm{H}\to\mathrm{L}} = \frac{\sqrt{\Lambda_{\mathrm{H}}\Lambda_{\mathrm{m}}}}{2\pi} \exp\left(S(X_{\mathrm{H}}) - S(X_{\mathrm{m}})\right), \tag{40b}$$

respectively, where the time rates $\Lambda_{\mathrm{L,\,m,\,H}}$ are evaluated as

$$\Lambda_{\mathrm{L,\,m,\,H}} = 2\left| X \frac{\partial \Lambda_X}{\partial X} \right| \quad \text{at} \quad X = X_{\mathrm{L,\,m,\,H}}. \tag{41}$$

Coefficients $\Lambda_{\mathrm{L,m,H}}$ are of the order unity, because the time rates are normalized. The transition rate dominantly comes from the exponential dependence on $S(X)$.

The transition rate is explicitly evaluated by use of the expression of the noise intensity equation (19). By use of equation (37), one has

$$S(X_{\mathrm{L}}) - S(X_{\mathrm{m}}) = -\Gamma K_{\mathrm{L}} \equiv -\Gamma \int_{X_{\mathrm{m}}}^{X_{\mathrm{L}}} \Lambda_X X \left(1 + UX^2\right)^2 \mathrm{d}X \,, \tag{42a}$$

$$S(X_{\mathrm{H}}) - S(X_{\mathrm{m}}) = -\Gamma K_{\mathrm{H}} \equiv -\Gamma \int_{X_{\mathrm{H}}}^{X_{\mathrm{m}}} \Lambda_X X \left(1 + UX^2\right)^2 \mathrm{d}X \,. \tag{42b}$$

Substitution of equation (42) into equation (40) provides the transition rate and back-transition rate as,

$$r_{\mathrm{L}\to\mathrm{H}} = \frac{\sqrt{\Lambda_{\mathrm{L}}\Lambda_{\mathrm{m}}}}{2\pi} \exp\left(-\Gamma K_{\mathrm{L}}\right), \tag{43a}$$

$$r_{\mathrm{H}\to\mathrm{L}} = \frac{\sqrt{\Lambda_{\mathrm{H}}\Lambda_{\mathrm{m}}}}{2\pi} \exp\left(-\Gamma K_{\mathrm{H}}\right), \tag{43b}$$

respectively.

Figure 8 illustrates the L-to-H-mode transition rate (solid line) and the back-transition rate (H-to-L-mode transition, dashed line) as a function of the pressure gradient. (Transition rates $r_{\mathrm{L}\to\mathrm{H}}$ and $r_{\mathrm{H}\to\mathrm{L}}$ are normalized to $\sqrt{\Lambda_L\Lambda_m}/2\pi$ and $\sqrt{\Lambda_H\Lambda_m}/2\pi$, respectively.) By substituting equations (15) and (42) into equation (43), the transition rates are numerically calculated and are shown in figure 8.

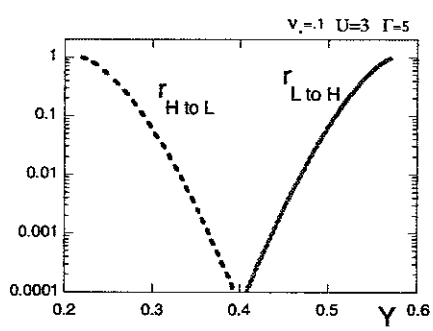

Figure 8 Transition probabilities $r_{\mathrm{L}\to\mathrm{H}}$ and $r_{\mathrm{H}\to\mathrm{L}}$ vs. pressure gradient. They are normalized to $\sqrt{\Lambda_L\Lambda_m}/2\pi$ and $\sqrt{\Lambda_H\Lambda_m}/2\pi$, respectively. (Other parameters are fixed as $U = 3$, $\Gamma = 5$ and $\nu_* = 0.1$.)

From figure 8 it is found following results. First, the transition rates become of the order of $\sqrt{\Lambda_L \Lambda_m}/2\pi$ or $\sqrt{\Lambda_H \Lambda_m}/2\pi$ near the ridge points. Second, the transition rates become of the order of 10^{-2} or 10^{-3} (measured in the units of $\sqrt{\Lambda_L \Lambda_m}/2\pi$ or $\sqrt{\Lambda_H \Lambda_m}/2\pi$) in the region where $r_{\mathrm{L}\to\mathrm{H}} \sim r_{\mathrm{H}\to\mathrm{L}}$ holds.

It is seen that owing to the statistical noise of micro-fluctuations, the transitions occur in a probabilistic manner. The life time (the staying time in one state) is given by the inverse of the transition rate,

$$\tau_{\mathrm{life}}^{\mathrm{L}\to\mathrm{H}} = 1 / r_{\mathrm{L}\to\mathrm{H}} . \tag{44}$$

4.4 Long time average and ensemble average

In a long time average, the probability that the state stays in the L-state is given as

$$P_{\mathrm{L}} = \frac{r_{\mathrm{H}\to\mathrm{L}}}{r_{\mathrm{L}\to\mathrm{H}} + r_{\mathrm{H}\to\mathrm{L}}} . \tag{45}$$

That for the H-state is given by

$$P_{\mathrm{H}} = \frac{r_{\mathrm{L}\to\mathrm{H}}}{r_{\mathrm{L}\to\mathrm{H}} + r_{\mathrm{H}\to\mathrm{L}}} . \tag{46}$$

The probability being in the H-mode is illustrated in figure 9 for the parameter of $\Gamma = 5$. It starts to increase when Y reaches the critical value of transition Y_{tran} . Then an exponential increase of the probability staying in the H-mode, P_H , is observed. For the case of figure 7, one observes $P_H \propto \exp\left(\left(Y - Y_{tran}\right)/\sigma_Y\right)$ and $\sigma_Y \simeq 0.038$. The width σ_Y is inversely proportional to the parameter Γ ; that is, $\sigma_Y \propto I_h^2 \propto \phi_{\mathrm{L}}^4$.

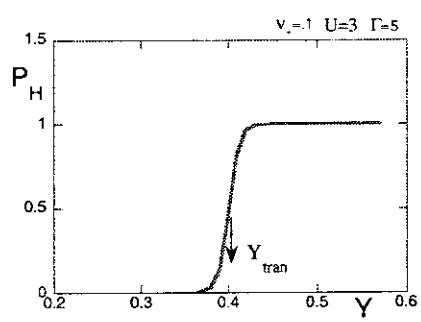

Figure 9 The probability being in the H-mode state for the case of figure 1 with fixed collision frequency $\nu_* = 0.1$. (Parameters are: $\alpha = 0.5$, $q = 3$, $\varepsilon = a/R = 1/3$, $U = 3$ and $\Gamma = 5$.)

The ensemble average of the electric field is expressed by the relation

$$\langle X \rangle = \int X P_{\rm eq}(X)\, {\rm d}X \ . \tag{47}$$

The ensemble average is equal to the long time average, and one has the evaluation from equations (45) and (46) as

$$\langle X \rangle = X_{\rm L} P_{\rm L} + X_{\rm H} P_{\rm H} \ . \tag{48}$$

This relation is alternatively derived if equation (47) is estimated by use of the method of the steepest descent. The Taylor expansions near $X \simeq X_{\rm L}$ and $X \simeq X_{\rm H}$ give the relations

$$S(X) \simeq \Lambda_{\rm L} g_X^{-2} \left(X - X_{\rm L}\right)^2 \ \text{and} \ S(X) \simeq \Lambda_{\rm H} g_X^{-2} \left(X - X_{\rm H}\right)^2 , \tag{49}$$

respectively. Substitution of equations (35) and (49) into equation (47) provides an estimate

$$\langle X \rangle = \frac{\sqrt{\Lambda_{\rm H}} \exp\left(-\Gamma K_{\rm H}\right) X_{\rm L} + \sqrt{\Lambda_{\rm L}} \exp\left(-\Gamma K_{\rm L}\right) X_{\rm H}}{\sqrt{\Lambda_{\rm H}} \exp\left(-\Gamma K_{\rm H}\right) + \sqrt{\Lambda_{\rm L}} \exp\left(-\Gamma K_{\rm L}\right)} \ , \tag{50}$$

which agrees with equation (48).

The ensemble average $\langle X \rangle$ is calculated for the case of figure 8, and is illustrated in figure 10. It is shown as a function of the pressure gradient Y for fixed value of

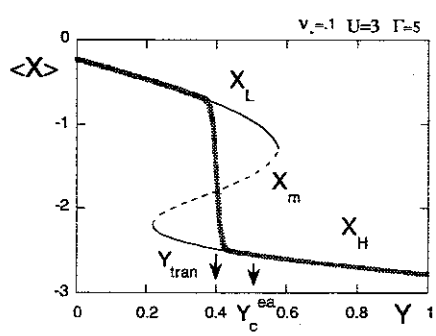

Figure 10 Statistical average of electric field as a function of the pressure gradient is shown by the thick solid line for fixed collision frequency $\nu_* = 0.1$. Thin solid line shows deterministic solution, $\Lambda_X X = 0$. $Y_{\rm tran}$ denotes the statistical phase limit, and $Y_{\rm c}^{\rm ea}$ denotes the condition of equal area where $\int J\, {\rm d}E$ vanishes. (Parameters are: $\alpha = 0.5$, $q = 3$, $\varepsilon = a/R = 1/3$, $U = 3$ and $\Gamma = 5$.)

collision frequency $\nu_* = 0.1$. The solution from the deterministic analysis, $\Lambda_X = 0$, is also shown by the thin line for the reference. Although a hysteresis exists in the deterministic solution, the ensemble average is a single-valued curve and does not exhibit the hysteresis. This is due to the statistical nature of transitions.

The statistical average $\langle X \rangle$ is a smooth function of Y in the vicinity of the critical transition point Y_{tran} . It is noted that the PDF of X has double peaks near $Y = Y_{\text{tran}}$. Apart from the ensemble average $\langle X \rangle$, the instantaneous value of X takes either X_{L} or X_{H} depending on the probabilities P_{L} and P_{H} . It fluctuates near the statistical average $\langle X \rangle$. Away from the transition region, the PDF $P_{\text{eq}}(X)$ has one dominant peak: the second peak exists but it is very small in the magnitude.

The ensemble average of the heat flux is calculated by substituting $X = \langle X \rangle$ into the relation of the heat flux equation (25) and is illustrated in figure 11. The statistical average in the long time limit of heat flux $\langle q_r \rangle$ as a function of the pressure gradient Y is shown by thick solid curve. Thin line (with hysteresis) indicates the result of deterministic theory. Thin dashed line indicates the collisional transport. (See figure 4.) The statistical average $\langle q_r \rangle$ does not show hysteresis, although the deterministic analysis predicts the hysteresis. The instantaneous value of q_r takes the value of either $q_r[X = X_{\text{L}}]$ or $q_r[X = X_{\text{H}}]$ near $Y = Y_{\text{tran}}$. This is because the PDF of X has double peaks in the vicinity of the transition region $Y = Y_{\text{tran}}$. Away from the transition region, the instantaneous value of q_r fluctuates near the statistical average $\langle q_r \rangle$.

4.5 Phase limit

The phase limit between the L- and H-modes in a control parameter space is obtained. The phase limit, on which the L-mode and H-mode have equal probability

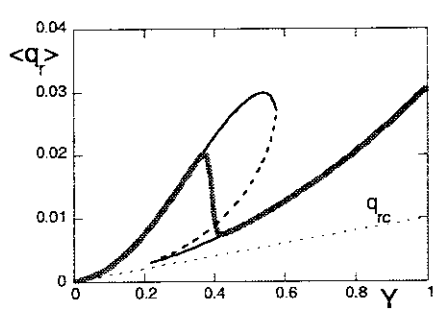

Figure 11 Statistical average of heat flux as a function of the pressure gradient. (Thick solid curve.) Thin line indicates the result of deterministic theory. Thin dashed line q_{rc} indicates the collisional transport. Heat flux in the vertical axis is measured in a unit of $c_s \ell^2 p_0 / 2Rq\rho_p$. (Parameters are: $\alpha = 0.5$, $q = 3$, $\varepsilon = a/R = 1/3$, $U = 3$ and $\Gamma = 5$.)

$P_L = P_H$, is given by the relation

$$r_{L\to H} = r_{H\to L} \,. \tag{51}$$

This condition is given from equation (43) as

$$S(X_H) = S(X_L) + \frac{1}{2}\ln\left(\Lambda_L/\Lambda_H\right). \tag{52}$$

Apart from a weak logarithmic dependence term, it is approximated as $S(X_H) = S(X_L)$, i.e.,

$$\int_{X_H}^{X_L} \Lambda_X X \left(1 + UX^2\right)^2 dX = 0 \,. \tag{53}$$

This result is an extension of the Maxwell's rule. When the noise is independent of X , the condition

$$\int_{X_H}^{X_L} \Lambda_X X \, dX = 0 \tag{54}$$

describes the phase limit. Noting that $\Lambda_X X$ is the normalized current, $\int \Lambda_X X \, dX$ corresponds to the usual work function $\int J \, dE$, and the Maxwell's rule is deduced. However, in far nonequilibrium systems like this turbulent plasma, the noise itself has the nonlinear dependence on X . The correction of UX^2 (illustrating the turbulence suppression) in the integrand is important in the H-mode $X \simeq X_H$. By this effect, the phase limit of ensemble average $\langle X \rangle$ deviates from the conventional criterion and the region of the H-mode becomes wider. The phase limit of the ensemble average equation (53) on (ν_b, Y) plane is shown in figure 12. The thick dashed line corresponds to Y_{tran} for the various value of ν_b . Thin dotted line indicates the equal-area condition Y_c^{ea} (Maxwell's rule) equation (54).

4.6 Observation of hysteresis

The observation of the hysteresis at the transition is determined by the competition between the transition rate and the rate of change of global plasma parameters. The presence of the statistical noise in the micro-fluctuations induces the transition and back-transition to occur in a probabilistic manner. As an average, the life time (the staying time in one state) is given by the inverse of the transition rate, $\tau_{life}^{L\to H} = 1 / r_{L\to H}$ or

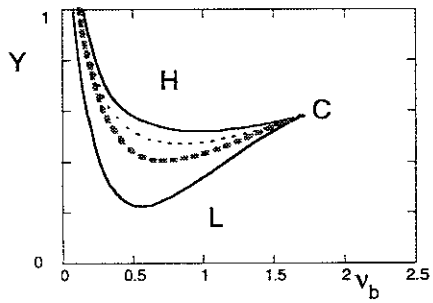

Figure 12 Phase diagram of the L-H transition. The solution of $\Lambda_X X = 0$ is characterized by the cusp catastrophe (thin line). 'C' denotes the critical point. Thick dashed line shows the phase boundary of ensemble average, equation (53). Thin dotted line indicates the equal-area condition (Maxwell's construction, equation (54)). (Parameters are: $\alpha = 0.5$, $q = 3$, $\varepsilon = a/R = 1/3$, $U = 3$ and $\Gamma = 5$.)

$\tau_{\rm life}^{\rm H\to L} = 1 / r_{\rm H\to L}$. When the characteristic time of the evolution of global parameters $\tau_{\rm global}$ is much longer than the life time, $\tau_{\rm global} >> \tau_{\rm life}$, two states are equilibrated by a large numbers of transitions. The probability that the state is found in one state is given by the long time average of many transitions. Therefore, it does not depend on from where the global parameters have evolved. In the case that $\tau_{\rm global}$ is in the range of life time, $\tau_{\rm global} \sim \tau_{\rm life}$, the probability that the state is found in one state strongly depends on from which branch the parameters have evolved, i.e., from the L-mode or from the H-mode. The hysteresis in the response to the global parameters is observed.

The condition $\tau_{\rm global} \sim \tau_{\rm life}$ depends on the absolute value of the difference of nonlinear potential. Statistically, the frequently enough number of transitions requires

$$r_{\rm L\to H} > \hat{\tau}_{\rm global}^{-1} , \tag{55}$$

i.e., $\exp\left(\Gamma K_{\rm L}\right) < \hat{\tau}_{\rm global}\sqrt{\Lambda_{\rm L}\Lambda_{\rm m}}\left(2\pi\right)^{-1}$. $(\hat{\tau}_{\rm global} = \tau_{\rm global} c_s/qR)$ This imposes an upper bound for Γ as

$$\Gamma K_{\rm L} < \ln\left(\hat{\tau}_{\rm global}\sqrt{\Lambda_{\rm L}\Lambda_{\rm m}}\left(2\pi\right)^{-1}\right) . \tag{56}$$

The coefficient Γ depends on the level of micro fluctuations as $\Gamma \propto I_h^{-2}$ in an L-mode plasma. This condition for Γ is evaluated as

$$\frac{\ell}{\sqrt{R\rho_i}} < \left(\frac{R}{a}\right)^{3/10}\left(\frac{\rho_i}{a}\right)^{1/10}\hat{\tau}_{ac}^{1/5}\,K_{\mathrm{L}}^{-1/5}\left|\ln\left(\hat{\tau}_{\mathrm{global}}\sqrt{\Lambda_{\mathrm{L}}\Lambda_{\mathrm{m}}}\,(2\pi)^{-1}\right)\right|^{1/5}, \qquad (57)$$

where a strong turbulence limit $\hat{\phi} = 1/\ell k_0$, together with estimates $k_0 \simeq 1/\ell_z \simeq 1/\rho_i$, is used. The integral I_{L} is of the order unity and logarithmic term is unimportant. Only a weak parameter dependence remains in the RHS of equation (57). The condition equation (57) is satisfied if the scale length ℓ belongs to a class of meso scale of $\sqrt{R\rho_i}$. It is noted that this scale length $\sqrt{R\rho_i}$ is much longer than micro scale lengths ρ_i and δ, so that the scale separation which is assumed in the beginning is validated.

5. Summary and discussion

In summary, the statistical theory of the E_r bifurcation in the edge of tokamak plasmas was analyzed. Micro fluctuations induce a random noise to the E_r-dynamics and the transition occurs in a probabilistic manner, if a deterministic model allows for more than one solution. The PDF for and the ensemble average of E_r were obtained. The rate of L/H transition was obtained, and a life-time of each state was calculated. The ensemble (statistical) average and the long time average were obtained. The effective phase limit of two states was given by the equal-probability condition for the H-and L-states. Owing to the suppression effect of turbulent noise by the shear in E_r, the limit was found to deviate from Maxwell's rule.

Implications to experiments are as follows: First, the cusp-boundaries of H-mode and the ensemble average of the transition condition in plasma parameters are different. They may show the different parameter dependences. They must be judged by both the ensemble averages of statistical models which have a noise source, and by a value of deterministic model. See figures 10 and 11. Due to the noise, each transition occurs being scattered around the ensemble average. This must be noticed in the future comparison of experimental database with many theories. Second, the ensemble averages of $\langle X \rangle$ and $\langle q_r \rangle$ do not show a hysteresis against global parameters Y, in contrast to the deterministic model. Third, the observation of hysteresis in experiments critically depends on the speed of global parameter change: this is another feature which characterizes the non-equilibrium properties. Fourth, the probabilistic onsets may change the occurrence of dithering between H-and L-states. Dynamical response in the presence of a model noise source has been studied in [29]. This theory gives a theoretical basis for the transition rates that governs the probabilistic occurrence of transitions.

In this article, the model of equation (15) was taken to show a typical example of probabilistic transition. Other mechanisms have been known to influence L-H transitions.[12] The inclusion of zonal flow excitation in statistical theory [17] or the

coupling of dynamics of different scale lengths [21] must be investigated for quantitative analysis of tokamak plasmas, and are left for future studies.

Acknowledgements

Authors wish to acknowledge Dr. M. Yagi, Dr. Y. Miura, Dr. A. Fujisawa, Dr. M. Kawasaki, Prof. A. Fukuyama and Prof. A. Yoshizawa for useful discussions. This work is partly supported by the Grant-in-Aid for Scientific Research of MEXT Japan and by the collaboration programmes of National Institute for Fusion Science and of the Research Institute for Applied Mechanics of Kyushu University.

REFERENCE

[1] Wagner F et al. 1982 Phys. Rev. Lett. **49** 1408;
ASDEX Team 1989 Nucl. Fusion **29** 1959

[2] Review of experimental observations of the H-mode and improved confinement states is given in, e.g., Itoh S-I, Itoh K and Fukuyama A 1995 *J. Nucl. Materials* **220-222** 117:
Burrell K H 1997 Phys. Plasmas **4** 1499;
Ida K 1998 Plasma Phys. Contr. Fusion **40** 1429;
Fujisawa A 2002 Plasma Phys. Contr. Fusion **44** A1

[3] Itoh S-I and Itoh K 1988 Phys. Rev. Lett. **60** 2276;
Itoh S-I and Itoh K 1989 Nucl. Fusion **29** 1031

[4] Shaing K C and Crume E Jr. 1989 Phys. Rev. Lett. **63** 2369

[5] Biglari H, Diamond P H, Terry P W 1990 *Phys. Fluids B* **2** 1

[6] Itoh S-I and Itoh K 1990 J. Phys. Soc. Jpn. **59** 3815

[7] Itoh K, Itoh S-I and Fukuyama A 1999 *Transport and Structural Formation in Plasmas* (IOP, England)

[8] Itoh S-I, Itoh K, Fukuyama A, Miura Y 1991 Phys. Rev. Lett. **67** 2485

[9] Hasegawa A and Wakatani M 1987 Phys. Rev. Lett. **59** 1581

[10] See, e.g.,
Diamond P H, Lebedev V B, Newman D E, Carreras B A, Hahm T S, Tang W M, Rewold G and Avinash K 1997 Phys. Rev. Lett. **78** 1472;
Malkov M A and Diamond P H 2001 Phys. Plasmas **8** 3996

[11] Terry P W 2000 Rev. Mod. Phys. **72** 109

[12] Yoshizawa A, Itoh S-I, Itoh K, Yokoi N 2002 Plasma Phys. Control. Fusion **43** R1

[13] Bowman J C, Krommes J A and Ottaviani M 1993 Phys. Fluids B **5** 3558

[14] Krommes J A 1999 Plasma Phys. Contr. Fusion **41** A641

[15] Itoh S-I and Itoh K 1999 J. Phys. Soc. Jpn. **68** 2611
[16] Itoh S-I and Itoh K 2000 J. Phys. Soc. Jpn. **69** 427
[17] Krommes J A and Kim C-B 2000 Phys. Rev. E. **62** 8508
[18] Miura Y, Ido T, Kamiya K, Hamada Y and JFT-2M Group 2001 Nucl. Fusion **41** 973
[19] Hugill J 2000 Plasma Phys. Contr. Fusion **42** R75
[20] Itoh S-I, Itoh K and Toda S 2002 "Probability of Statistical L-H Transition in Tokamaks" Phys. Rev. Lett. **88** in press.
[21] Itoh S-I and Itoh K 2001 Plasma Phys. Contr. Fusion **43** 1055
[22] Itoh S-I, Itoh K, Yagi M, Kawasaki M and Kitazawa A 2002 Phys. Plasmas **9** 1947
See, also Itoh S-I, Kitazawa A, Yagi M and Itoh K 2002 Plasma Phys. Contr. Fusion **44** 1311
[23] Kraichnan R H 1970 J. Fluid Mech. **41** 189
[24] Kim J, Burrel K H, Gohil P, Groebner R J, Kim Y -B, John H E St., Seraydarian R P and Wade M R 1994 Phys. Rev. Lett. **72** 2199
[25] Stringer T E 1993 Nucl. Fusion **33** 1249
[26] Diamond P H, Liang Y -M, Carreras B A, Terry P W 1994 Phys. Rev. Lett. **72** 2565.
[27] Rozhanskii V, Tendler M 1992 Phys. Fluids B **4** 1877
Sugama H, Horton C W 1995 Plasma Phys. Contr. Fusion **37** 345
[28] Kawasaki M, Furuya A, Yagi M, Itoh K, Itoh S -I 2002 Plasma Phys. Contr. Fusion **44** A473
[29] Itoh S-I, Toda S, Yagi M, Itoh K, Fukuyama A 1998 Plasma Phys. Contr. Fusion **40** 737;
Toda S, Itoh S-I, Yagi M, Itoh K, Fukuyama A 1999 J. Phys. Soc. Jpn. **68** 3520